Science Advances
AAAS

# Supplementary Materials for

## Dynamic instability of dendrite tips generates the highly branched morphologies of sensory neurons

Sonal Shree *et al.*

Corresponding author: Jonathon Howard, joe.howard@yale.edu

*Sci. Adv.* **8**, eabn0080 (2022)
DOI: 10.1126/sciadv.abn0080

**The PDF file includes:**

Figs. S1 to S9
Tables S1 to S3
Legends for movies S1 to S10
References

**Other Supplementary Material for this manuscript includes the following:**

Movies S1 to S10

## Supplementary Figures

### Figure S1: Definitions of the axes, the coverage index and neuronal growth controls

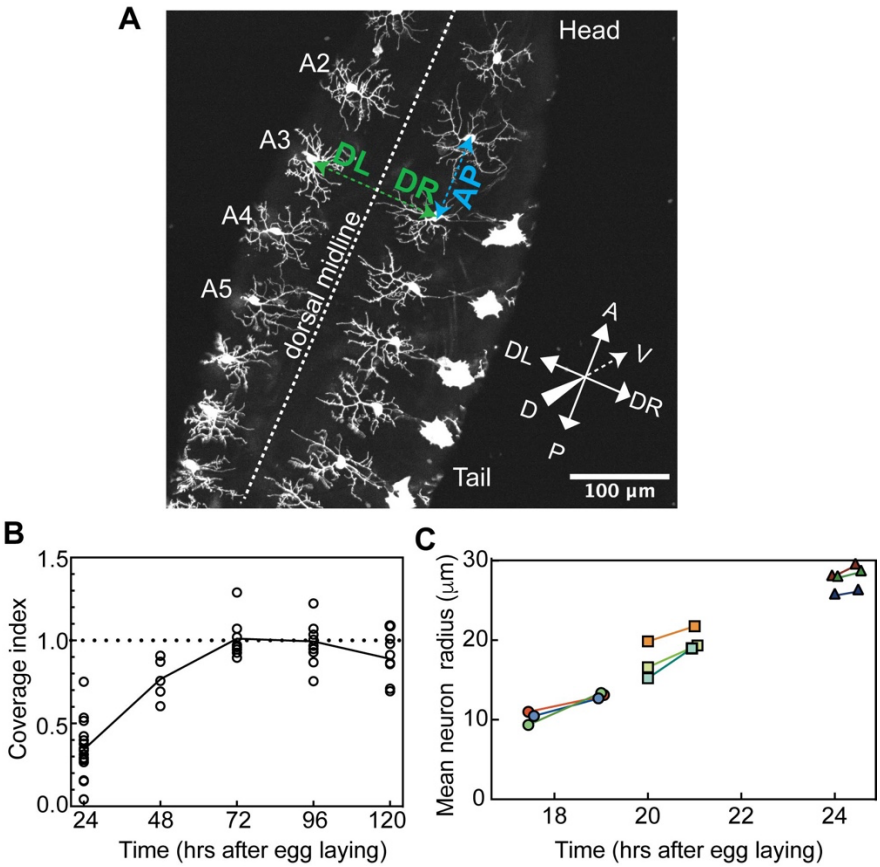


**A** Definitions of the anterior-posterior (AP) and dorsal left (DL) and dorsal right (DR) axes. This larva was imaged from the dorsal side up, which was adjacent to the coverslip surface closest to the objective. A2, A3, A4, and A5 correspond to the dorsal abdominal segments. The white dashed line is the dorsal midline. This larva is ~24 hr after egg lay (genotype - ;;ppkCD4-tdGFP). The AP length was measured as the distance between the cell bodies of the adjacent neurons on the anterior and posterior sides. The DL-DR length was measured as the distance between cell bodies in adjacent hemisegments (across the midline) corrected for the offset of the cell bodies, which are not in the centers of the cells but displaced away from the midline. For sake of simplicity, we are calling DL-DR as LR **B** The coverage index over development time ($n \geq 5$ neurons). The coverage index is calculated as the ratio the dendrite area (AP cell width x LR cell width, from Figure 1D) divided by the dorsal hemisegment area (AP hemisegment width x LR hemisegment, width from Figure 1D). **C** Control showing that imaging does not perturb growth**.** The growth of cells was assessed by measuring the cell radius (calculated as √(area/π)) over time. Lines connect cells at the beginning and end of imaging. This shows that the imaging conditions do not retard growth.

## Figure S2: Tracking dendrite tips

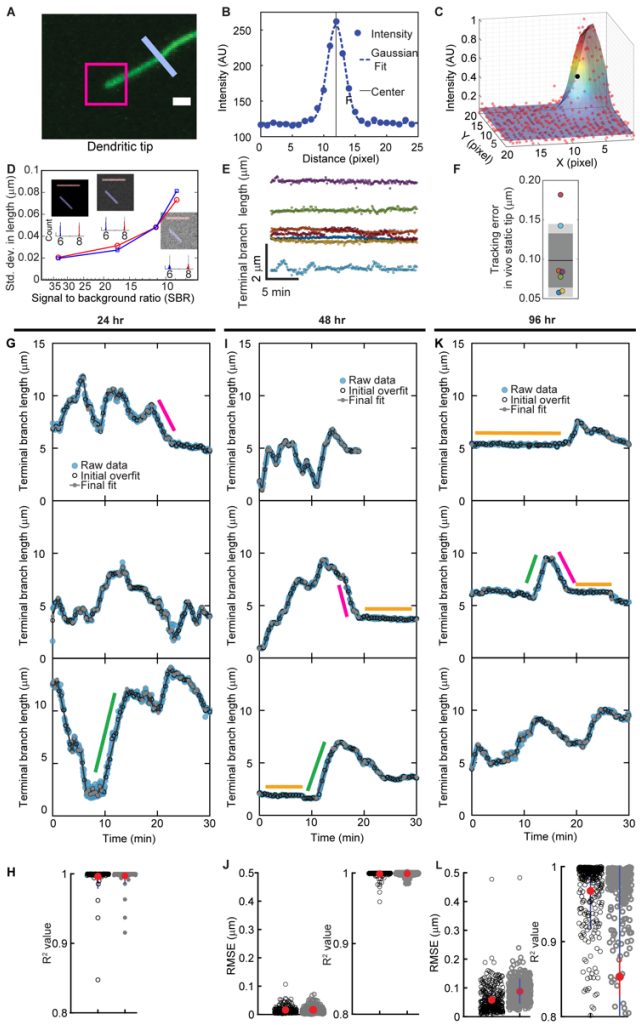


**A** Example of a fluorescently labeled terminal dendrite. **B** The center of the dendrite was located by fitting the cross-sections (blue line in B) to a Gaussian. The precision is approximately 0.1 μm. **C** The position of the tip of the dendrite was calculated by fitting the end intensity profile (magenta box in A) to a 2D function corresponding to a Gaussian in the perpendicular direction and an error function the parallel direction (see Methods) **D** Montage of simulated images of cylindrical tubes (6 μm blue, 8 μm red) that are fluorescently labeled with 10% labeling density on the surface with signal-to-background ratio (SBR), defined as the mean signal divided by the standard deviation of background noise, varying from 33 (left) to 9 (right). The pixel size is 100 nm. The measured length distribution is shown in the bottom panel (200 independently generated images for each SBR). **E** The lengths of several live-imaged dendrites that were in their paused state as a function of time. **F** The standard deviation of the measured lengths in E is shown. The accuracy is high even for live imaging condition. **G** The standard deviation of the tracked lengths is ~1 pixel (108 nm). Examples of tracked dendritic length as a function of time: **G** 24 hr. **I** 48 hr. and **K** 96 hr. The green, orange, and magenta lines denote examples of growing, paused, and shrinking states. The tips tend to spend more time in the paused state over developmental time. **H**, **J**, and **L** show the statistics of the piecewise-linear fitting.

**Figure S3: Correlation between state velocities and lifetimes and state durations.**

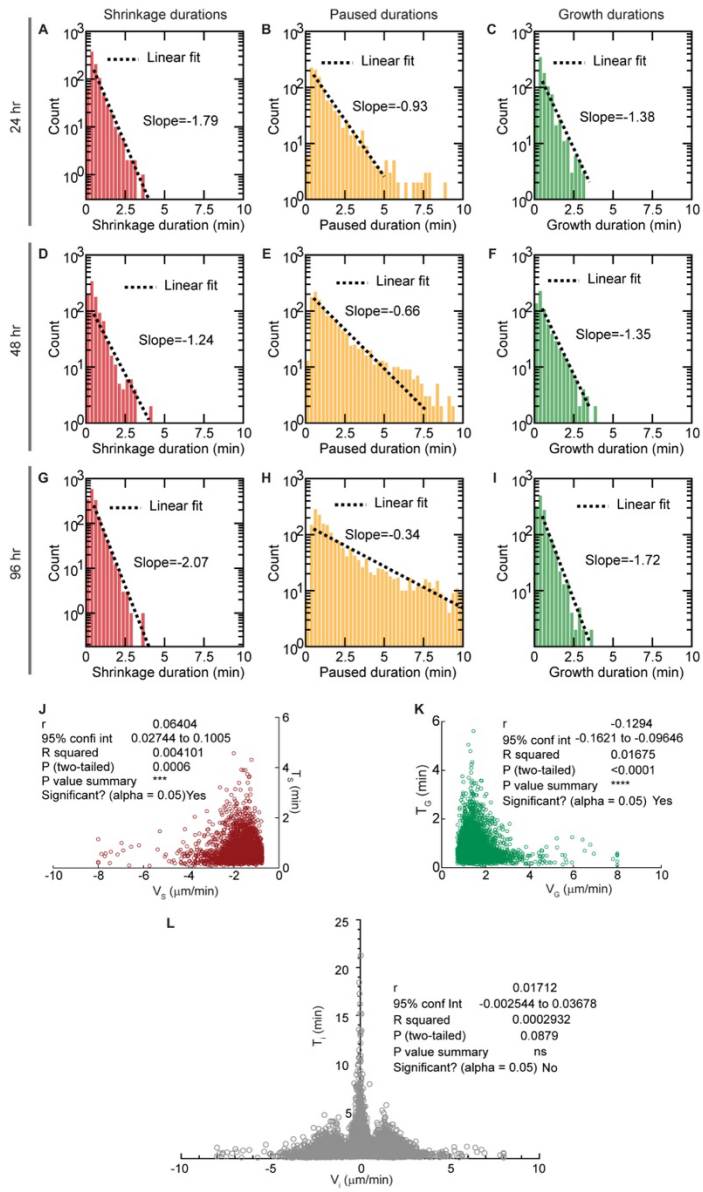


The distribution durations for the shrinking (S), paused (P), and growing (G) states at 24 hr (**A-C**), 48 hr (**D-F**), and 96 hr (**G-I**) plotted using semi-log axes. The distributions are very close to exponentials (dotted lines) expected if switching among the states is first order. The slope of the dotted lines is the inverse of the lifetimes spent in the states: for example, at 24 hr, the sum of the transition rates from growing state is ($K_{\mathrm{GP}} + K_{\mathrm{GS}} = 0.696 + 0.509 = 1.205$ min$^{-1}$ (Table 1 A), close to the slope of the lifetime distribution of 1.38 min$^{-1}$ (F). **J** The correlation between shrinking velocities ($V_{\mathrm{S}}$) and shrinking lifetimes ($T_{\mathrm{S}}$) shows a significant correlation with Pearson's correlation coefficient $r$=0.064. **K** Similarly, a significant correlation is observed between growth velocities ($V_{\mathrm{G}}$) and growth lifetimes ($T_{\mathrm{G}}$)**. L** Pearson's correlation coefficient ($r$) between state velocities ($V_i$) and lifetimes ($T_i$) for 18-20 hr data. The value of $r$ is small (0.017) and there is no significant correlation between $V_i$ and $T_i$.

**Figure S4: Evidence for persistent growth after birth.**

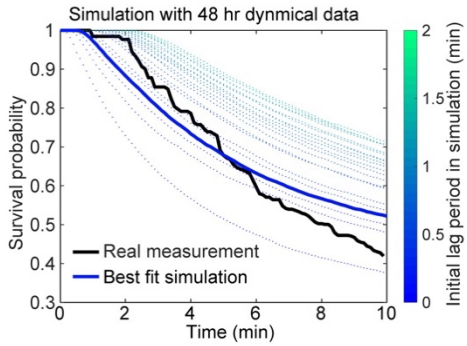


We manually measured the time between branch initiation and branch death at different stages of the larva (24, 48,72, and 96 hr AEL, 3 movies for each stage). From these data, we calculated the survival probability by dividing the number of alive branches by the total number of branches using the formula described in the Methods. The black line is the average survival probability of the real dendrite tips. The survival probability does not start decaying exponentially as one might expect if it were a Poisson process. Rather, it shows some initial lag. This observation led us to believe that branch initiation is not a simple Poisson process. To estimate the initial lag period, we simulated 1000 branches with initial length 0.5 μm and implemented a lag time ($\tau_{lag}$) by preventing the tips to switch into the paused or shrinkage state ( $K_{GP} = K_{GS} = 0; t \leq \tau_{lag}$). A branch is deleted in the simulation when its length is <0.1 μm. The survival probability increases with the initial lag τ as shown by the dotted lines. The dark blue is the best fit to the real data ( $\tau_{lag}$ = 0.3 min).

**Figure S5**: **Sensitivity of morphology to branching and growth parameters**.

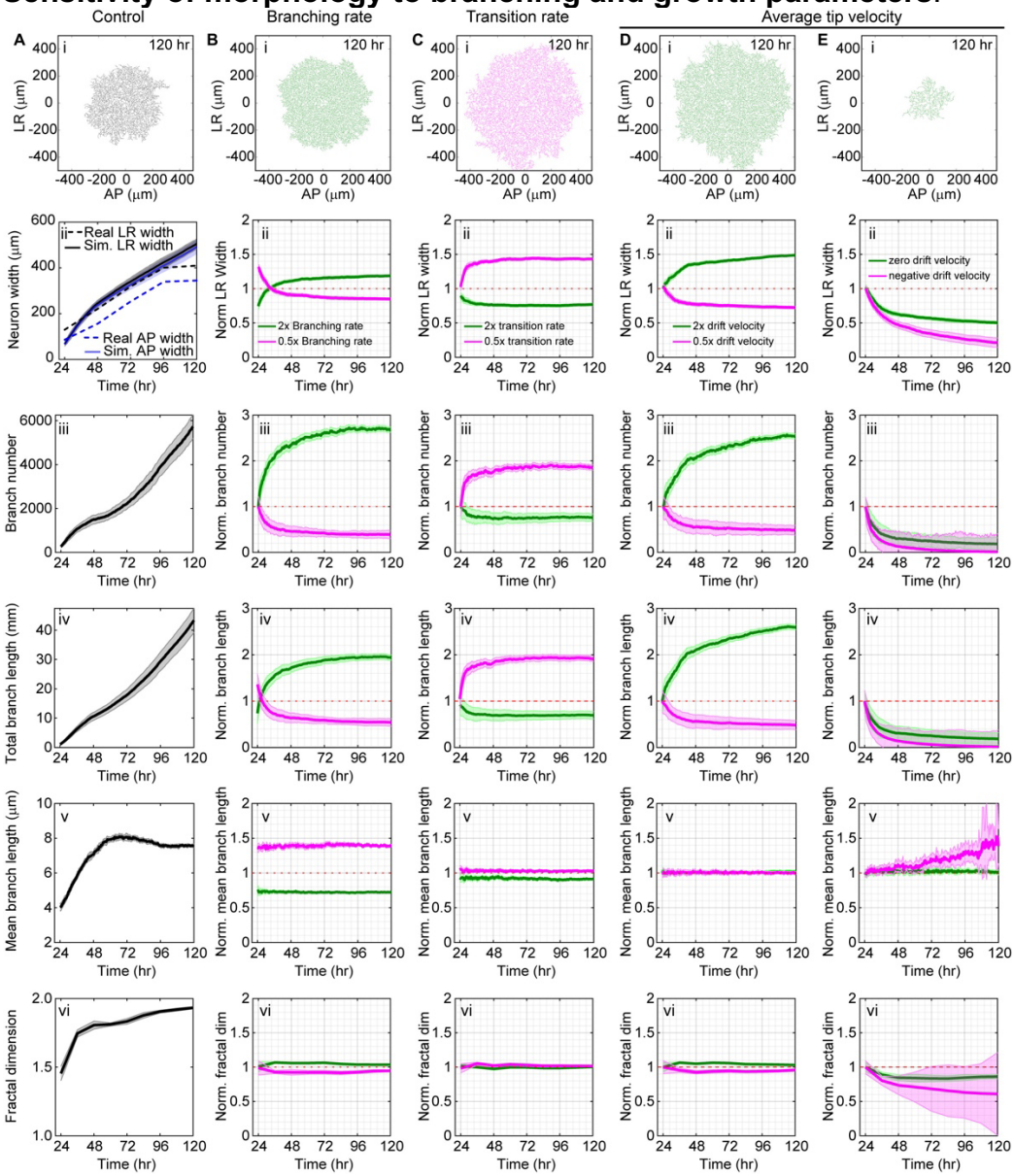


**A** Control with parameters from Table 1 and Tables S1-2 without any boundary restriction. The black and blue dashed lines represent LR and AP widths respectively. The solid lines represent the simulated segment sizes over development. The simulation shows that initially (24-48 hr) the neurons grow faster than the real segment and then grow with a constant rate equal to the segment growth rate (~0.06 μm/min) until 96 hr. The segment widths saturate after 96 hr even without a boundary. **B** Branching rate was doubled (green) and halved (magenta) compared to the control, keeping all other parameters unchanged. All arbor properties are normalized by the respective unconstrained controls. Fold change is plotted against time for (ii) arbor size, (iii) branch number, (iv) branch length, (v) mean branch length, and (vi) fractal dimension. **C** All transition rates were doubled (green) and halved (magenta): this leads to a decrease and increase in the variability of growth. **D** The mean tip velocity (drift) was increased (green) and decreases (magenta) 2-fold. **E** The average (drift) velocity was set to zero (green) and a negative value (-0.02 /min, magenta). Shaded regions represent standard error of mean.

**Figure S6**: **Branch length and radial orientation distributions**.

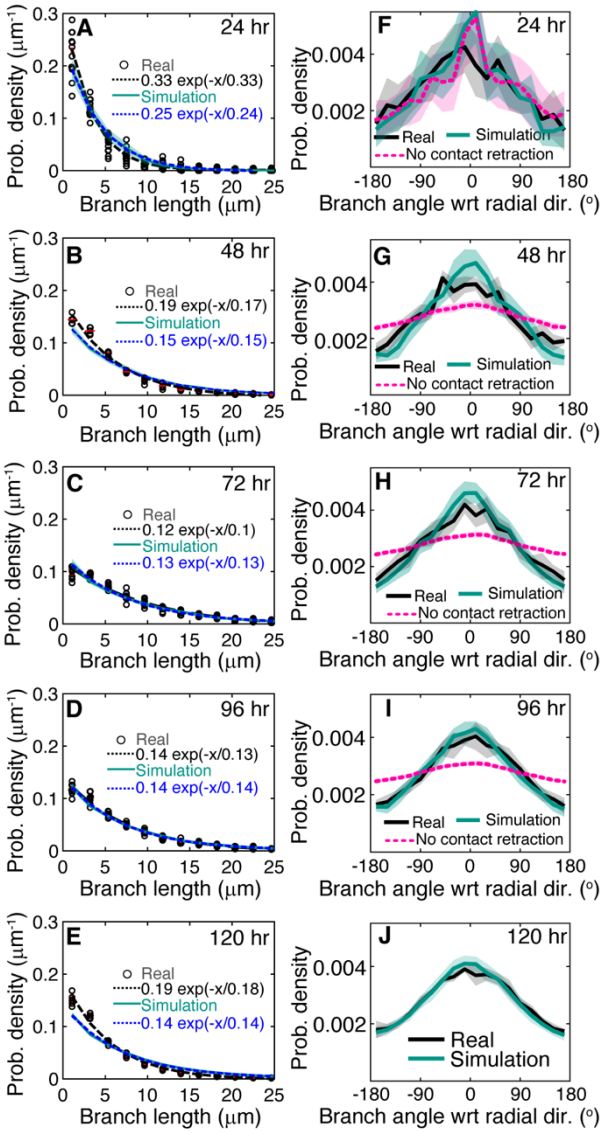


**A-E** Branch length distribution over different developmental stages for real and simulated arbors with exponential fits (dashed lines). **F-J** Radial orientation of branches over developmental time for real and simulated arbors. The branches are preferentially oriented in the radial direction. This preference is due to contact-based retraction. The dotted curves show diminished radial preference when branches are paused after contact in the simulation. Shades represents standard deviations.

## Figure S7: Branching drives arbor expansion when the net tip growth is zero

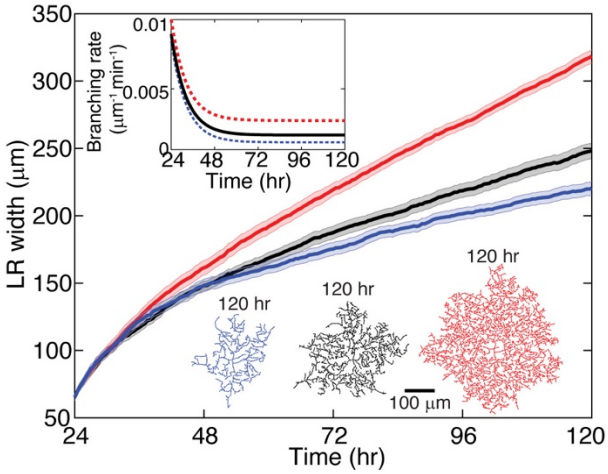


To understand the relationship between the short-term dynamics (the growth-shrink-pause dynamics including branching) and the long-term formation of stable branches, we explored our simulation keeping the net growth of tips at zero (meaning there is no net growth from G-P-S dynamics) and varied the branching rate (as shown by the red, black and blue lines in the top inset). We observed, even for zero net growth, that the dendritic arbor grows in size as shown by the LR widths (different colored arbors correspond to the differently colored branching rates in the top inset). The bottom panel shows the color-coded final arbor sizes.

## Figure S8: Generalization of our model to other systems

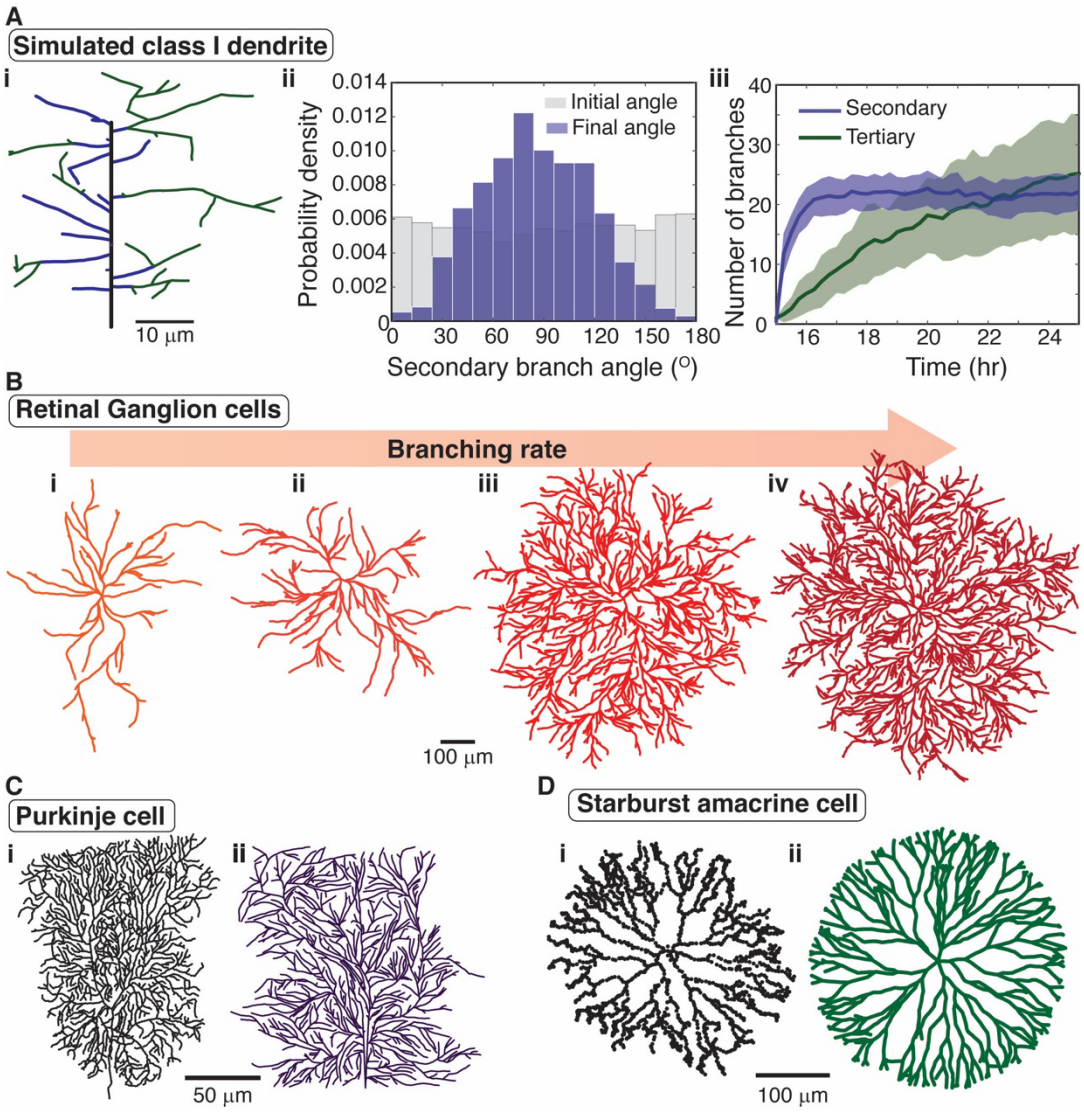


**A** (i) A representative simulated *Drosophila* class-I dendrite at 25 hr. Class-I dendrites were simulated by initializing the model with a single static primary branch and then allowing branching from primary and secondary branches with rates $0.05\exp(-t/5) + 0.005\ \mu\mathrm{m}^{-1}\mathrm{min}^{-1}$ and $0.005\exp(-t/5) + 0.0005\ \mu\mathrm{m}^{-1}\mathrm{min}^{-1}$) respectively, where $t$ is time in hrs. (ii) The simulation recapitulates one of the key findings in (*33*) namely that the secondary branches are orthogonal to the primary branch (blue histogram peaking around 90°) even though the initial angles were uniformly distributed (gray). This is a consequence of contact-based retraction. (iii) The number of secondary and non-secondary branches approaches 22 and 30 at long times respectively, in accordance with data from (*33*). **B** Different retinal ganglion cells were simulated using different branching rates and a small branching angle (45° relative to the direction of the mother). The morphologies are similar to those of marmoset retinal ganglion cells (*75*). **C** A real Purkinje cell (i) ((*76*), raw data downloaded from NeuroMorpho.org) was simulated using slow growth of dendritic tips and complete retraction after contact to recapitulate the locally parallel branch orientations (ii). **D** An example of a real starburst amacrine cell (i) ((*77*), raw data downloaded from NeuroMorpho.org) and a simulated cell (ii) in which it was necessary to replace lateral branching with tip bifurcation to recapitulate the observed morphology.

**Figure S9: Validation of trajectory analysis method**.

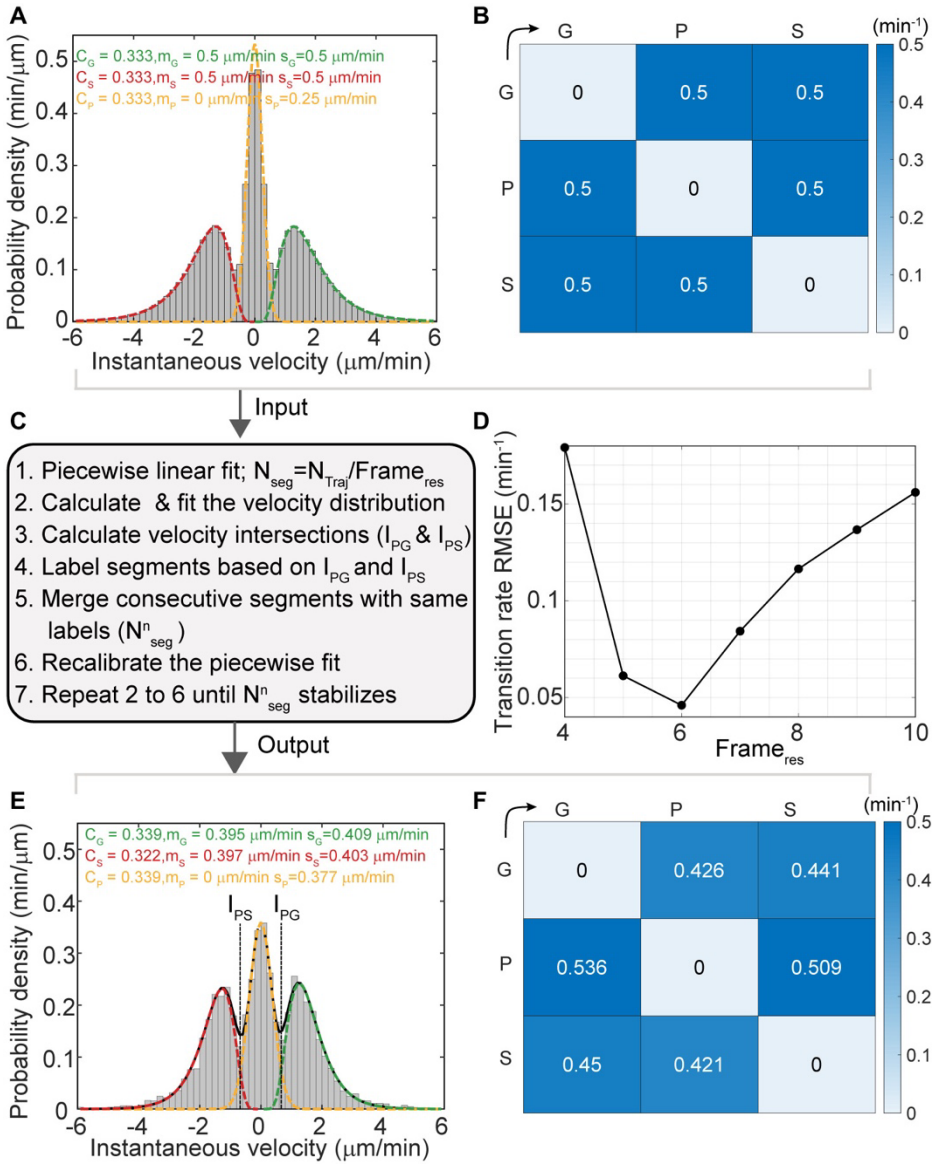


We simulated 200 Markov trajectories with realistic input parameters shown in **A** and **B** and then added Gaussian white noise on the individual points of the trajectories. We used the transition rate as 0.5 /min because of the observed fact that the individual states last ~1 minute. **C** The flowchart of the trajectory analysis method. **D** We varied the Frame resolution to find the optimal resolution. The root-mean-squared error between the input and output transition rate matrix is plotted as a function of frame resolution. Frame resolution of 6 provides the best result and we chose this value for all our analyses. **E** &**F** The output velocity distribution and transition rate matrix using frame resolution 6. Our method of analysis produced a faithful reproduction of the input parameters.

# Supplementary Tables

## Table S1: Branching rates

| Age (hr) | Total branching rate[a] ($min^{-1}$) (Mean ± SD) | Linear branching rate[b] ($\mu m^{-1} \cdot min^{-1}$) (Mean ± SD) | Branching angle[c] (°) (Mean ± SD) | Numbers (rates, angles) |
|---|---|---|---|---|
| 18 (E) | 4.26 ± 0.59 | 0.0109 ± 0.0015 | 85 ± 25 | $n = 9, 5$ |
| 24 (L1) | 7.59 ± 1.52 | 0.0095 ± 0.0017 | 88 ± 26 | $n = 9, 7$ |
| 36 (L1) | 5.77 ± 2.67 | 0.0031 ± 0.0009 | 85 ± 25 | $n$ = 6,7 |
| 48 (L2) | 4.86 ± 1.59 | 0.0019 ± 0.0007 | 86 ± 26 | $n$ = 6,4 |
| 72 (L2) | 8.31 ± 2.37 | 0.0011 ± 0.0004 | 90 ± 25 | $n$ = 6,5 |
| 96 (L3) | 11.12 ± 2.52 | 0.0011 ± 0.0006 | 91 ± 25 | $n$ = 6,4 |

[a]Over the entire dendrite arbor
[b]Per total dendrite length
[c]Angle between dendrites is zero in the distal direction of the mother.
Standard deviation (SD).

## Table S2: Model parameters

| Name | Description | Value |
|---|---|---|
| $l_{\text{initial}}$ | Initial length of nascent branch | 0.50 μm |
| $l_{\text{interaction}}$ | Length scale of contact | 0.15 μm |
| $\tau_{\text{post-contact}}$ | Post-contact dynamics duration | 15 min |
| $\tau_{\text{lag}}$ | Initial lag of nascent branch | 0.3 min |
| $l_{\text{P}}$ | Persistence length | 150 μm |
| $R_{\text{soma}}$ | Radius of soma | 10 μm |
| $\mu_b^\theta$ | Mean branching angle | $\pi/2$ |
| $\sigma_b^\theta$ | Standard dev. of branching angle | $\pi/7$ |

## Table S3: Mutations and morphologies

| Mutation | Reference | Morphology | Features of mutants accounted for by the model | Simulated neuron | Parameters |
|---|---|---|---|---|---|
| **Non-uniform branching** | | | | | |
| Dynein intermediate light chain (Dlic) | (*21*, *22*, *64*) | 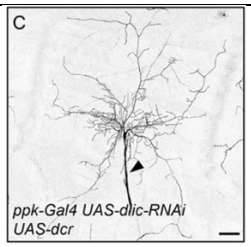  Fig 2C (*64*) | Downsizing of the overall arbor, arbors fail to fill the hemisegment. More branches in the proximal region. * |  | Non uniform branching, primary branch has basal branching rate. |
| Lis-1 | (*21*, *22*, *78*) | 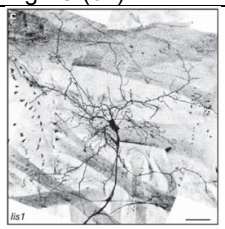  Fig 1C (*22*) | Downsizing of the overall arbor, arbors fail to fill the hemisegment. * | | |
| **Change in tip dynamics** | | | | | |
| katanin | (*24*) | 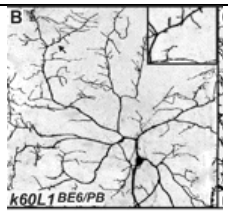  Fig 3B (*24*) | Decreased dendritic branch number, length and density. | 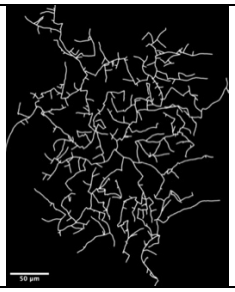 | Terminal branches spend less time in the paused state and more time in the shrinking state. |
| **Self-avoidance** | | | | | |
| Trc | (*15*) | 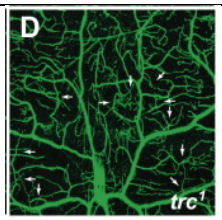  Arrows represent dendrites crossovers Fig 1D (*15*) | More branches and branch crossovers. * | 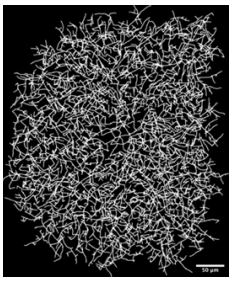 | Branches are allowed to cross 10 % of the time. |
| Dscam | (*11*–*13*) | 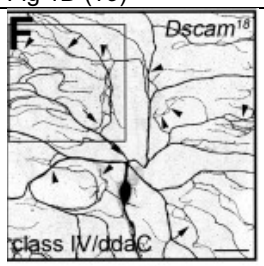  Arrows represent dendrite crossovers Fig 1F (*13*) | More branches and branch crossovers. * | | |

*Mutants display additional phenotypes not accounted for in the model.

# Supplementary movies

## Movie S1. Time-lapse movie of a growing neuron:

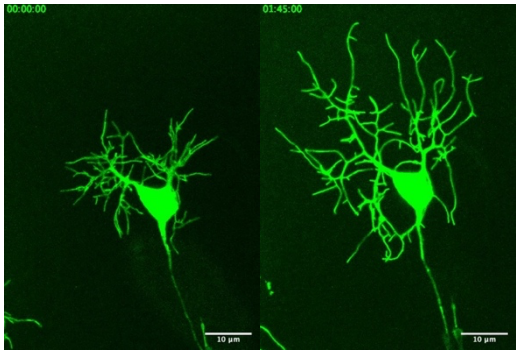


Time lapse movie of a fast embryonic neuronal growth at 17.5hr AEL was acquired using a spinning disk confocal microscope. The movie was full-frame (2048x 2048 pixels) and a complete stack of images (7um) was produced every 5 mins interval. Genotype of embryo was *;;ppkCD4-tdGFP* .

**Movie S2. Tip growth and branching:** Time lapse movie at 24hr AEL was acquired using a spinning disk confocal microscope. A cropped stack of images (7um) was produced every 5 seconds interval. Genotype of larva was *;;ppkCD4-tdGFP* .

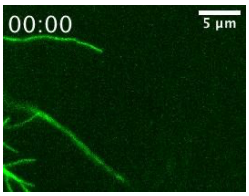


Example of dendrite tip growth and branching

**Movie S3. Self-avoidance and shrinkage:** Time lapse movie at 24hr AEL were acquired using a spinning disk confocal microscope. A cropped stack of images (7um) was produced every 5 seconds interval. Genotype of larva was *;;ppkCD4-tdGFP* .

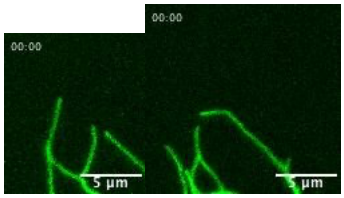


Example of contact-based retraction

**Movie S4. Self-avoidance and growth:** Time lapse movie at 24hr AEL was acquired using a spinning disk confocal microscope. A cropped stack of images (7um) was produced every 5 seconds interval. Genotype of larva was *;;ppkCD4-tdGFP* .

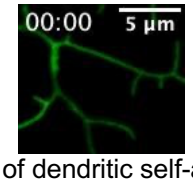


Example of dendritic self-avoidance

**Movie S5. Tip pause:** Time lapse movie at 24hr AEL was acquired using a spinning disk confocal microscope. A cropped stack of images (7um) was produced every 5 seconds interval. Genotype of larva was *;;ppkCD4-tdGFP* .

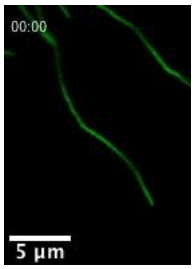


Example of a tip going into a paused state

**Movie S6-10. Tip growth, bending, and branching**.

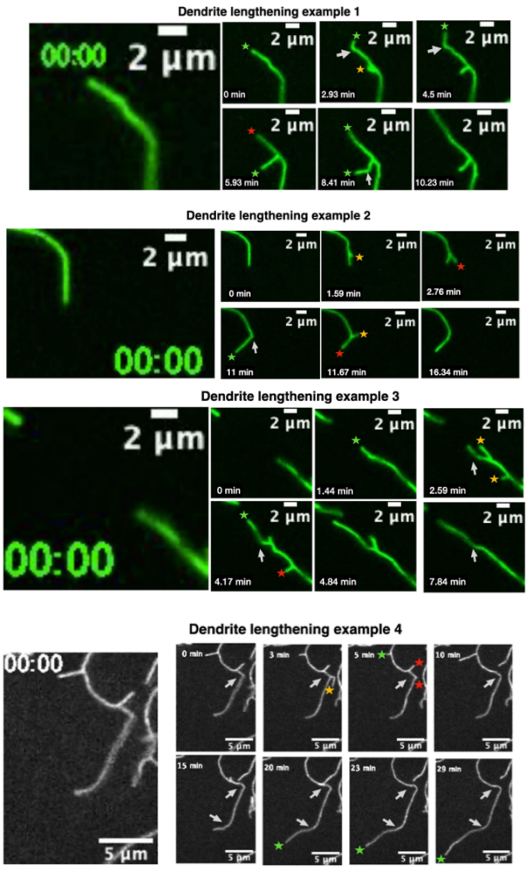

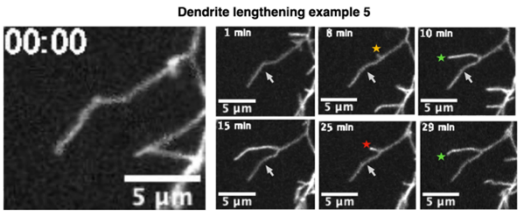


Dendrite lengthening is likely due to the addition of materials at the dendrite tip. The green stars show dendrite tip lengthening, the yellow star is birth of new branch, and the red star is a shrinkage event. White arrows point to the bending of growing tips. In example two, where the branch disappears, a sharp bend smoothens over time. In examples 3,4, and 5, the white arrows correspond to structural features such as branches and bends that remain fixed during growth and shortening. All time lapse movies shown above were acquired from different 24hr larvae using spinning disk confocal. Genotype of all larvae were *;;ppkCD4-tdGFP* .

## REFERENCES AND NOTES


1. S. Ramón y Cajal, The structure and connexions of neurons, *Nobel Lecture* (1906).

2. J. L. Lefebvre, J. R. Sanes, J. N. Kay, Development of dendritic form and function. *Annu. Rev. Cell Dev. Biol.* **31**, 741–777 (2013).

3. A. Fornito, A. Zalesky, M. Breakspear, The connectomics of brain disorders. *Nat. Rev. Neurosci.* **16**, 159–172 (2015).

4. Z. Zheng, J. S. Lauritzen, E. Perlman, C. G. Robinson, M. Nichols, D. Milkie, O. Torrens, J. Price, C. B. Fisher, N. Sharifi, S. A. Calle-Schuler, L. Kmecova, I. J. Ali, B. Karsh, E. T. Trautman, J. A. Bogovic, P. Hanslovsky, G. S. X. E. Jefferis, M. Kazhdan, K. Khairy, S. Saalfeld, R. D. Fetter, D. D. Bock, A complete electron microscopy volume of the brain of adult *Drosophila melanogaster*. *Cell* **174**, 730–743.e22 (2018).

5. W. Denk, K. L. Briggman, M. Helmstaedter, Structural neurobiology: Missing link to a mechanistic understanding of neural computation. *Nat. Rev. Neurosci.* **13**, 351–358 (2012).

6. E. T. Stoeckli, Understanding axon guidance: Are we nearly there yet? *Development* **145**, dev151415 (2018).

7. Y.-N. Jan, L. Y. Jan, Branching out: Mechanisms of dendritic arborization. *Nat. Rev. Neurosci.* **11**, 316–328 (2010).

8. A. Singhania, W. B. Grueber, Development of the embryonic and larval peripheral nervous system of *Drosophila*. *Wiley Interdiscip. Rev. Dev. Biol.* **3**, 193–210 (2014).

9. R. Basak, S. Sutradhar, J. Howard, Focal laser stimulation of fly nociceptors activates distinct axonal and dendritic $Ca^{2+}$ signals. *Biophys. J.* **120**, 3222–3233 (2021).

10. J. L. Robertson, A. Tsubouchi, W. D. Tracey, Larval defense against attack from parasitoid wasps requires nociceptive neurons. *PLOS ONE* **8**, e78704 (2013).

11. M. E. Hughes, R. Bortnick, A. Tsubouchi, P. Bäumer, M. Kondo, T. Uemura, D. Schmucker, Homophilic Dscam interactions control complex dendrite morphogenesis. *Neuron* **54**, 417–427 (2007).

12. B. J. Matthews, M. E. Kim, J. J. Flanagan, D. Hattori, J. C. Clemens, S. L. Zipursky, W. B. Grueber, Dendrite self-avoidance is controlled by Dscam. *Cell* **129**, 593–604 (2007).

13. P. Soba, S. Zhu, K. Emoto, S. Younger, S.-J. Yang, H.-H. Yu, T. Lee, L. Y. Jan, Y.-N. Jan, Drosophila sensory neurons require Dscam for dendritic self-avoidance and proper dendritic field organization. *Neuron* **54**, 403–416 (2007).

14. J. Z. Parrish, P. Xu, C. C. Kim, L. Y. Jan, Y. N. Jan, The microRNA bantam functions in epithelial cells to regulate scaling growth of dendrite arbors in Drosophila sensory neurons. *Neuron* **63**, 788–802 (2009).

15. K. Emoto, Y. He, B. Ye, W. B. Grueber, P. N. Adler, L. Y. Jan, Y.-N. Jan, Control of dendritic branching and tiling by the tricornered-kinase/furry signaling pathway in Drosophila sensory neurons. *Cell* **119**, 245–256 (2004).

16. W. B. Grueber, B. Ye, A. W. Moore, L. Y. Jan, Y. N. Jan, Dendrites of distinct classes of Drosophila sensory neurons show different capacities for homotypic repulsion. *Curr. Biol.* **13**, 618–626 (2003).

17. S. Jinushi-Nakao, R. Arvind, R. Amikura, E. Kinameri, A. W. Liu, A. W. Moore, Knot/collier and cut control different aspects of dendrite cytoskeleton and synergize to define final arbor shape. *Neuron* **56**, 963–978 (2007).

18. C. Han, D. Wang, P. Soba, S. Zhu, X. Lin, L. Y. Jan, Y. N. Jan, Integrins regulate repulsion-mediated dendritic patterning of drosophila sensory neurons by restricting dendrites in a 2D space. *Neuron* **73**, 64–78 (2012).

19. M. E. Kim, B. R. Shrestha, R. Blazeski, C. A. Mason, W. B. Grueber, Integrins establish dendrite-substrate relationships that promote dendritic self-avoidance and patterning in Drosophila sensory neurons. *Neuron* **73**, 79–91 (2012).

20. T. Stürner, A. Tatarnikova, J. Mueller, B. Schaffran, H. Cuntz, Y. Zhang, M. Nemethova, S. Bogdan, V. Small, G. Tavosanis, Transient localization of the Arp2/3 complex initiates neuronal dendrite branching in vivo. *Development* **146**, dev171397 (2019).

21. D. Satoh, D. Sato, T. Tsuyama, M. Saito, H. Ohkura, M. M. Rolls, F. Ishikawa, T. Uemura, Spatial control of branching within dendritic arbors by dynein-dependent transport of Rab5-endosomes. *Nat. Cell Biol.* **10**, 1164–1171 (2008).

22. Y. Zheng, J. Wildonger, B. Ye, Y. Zhang, A. Kita, S. H. Younger, S. Zimmerman, L. Y. Jan, Y. N. Jan, Dynein is required for polarized dendritic transport and uniform microtubule orientation in axons. *Nat. Cell Biol.* **10**, 1172–1180 (2008).

23. N. T. Sherwood, Q. Sun, M. Xue, B. Zhang, K. Zinn, Drosophila spastin regulates synaptic microtubule networks and is required for normal motor function. *PLOS Biol.* **2**, e429 (2004).

24. A. Stewart, A. Tsubouchi, M. M. Rolls, W. D. Tracey, N. T. Sherwood, Katanin p60-like1 promotes microtubule growth and terminal dendrite stability in the larval class IV sensory neurons of Drosophila. *J. Neurosci.* **32**, 11631–11642 (2012).

25. K. M. Ori-McKenney, L. Y. Jan, Y.-N. Jan, Golgi outposts shape dendrite morphology by functioning as sites of acentrosomal microtubule nucleation in neurons. *Neuron* **76**, 921–930 (2012).

26. G. A. Ascoli, J. L. Krichmar, L-neuron: A modeling tool for the efficient generation and parsimonious description of dendritic morphology. *Neurocomputing* **32-33**, 1003–1011 (2000).

27. S. Nanda, R. Das, S. Bhattacharjee, D. N. Cox, G. A. Ascoli, Morphological determinants of dendritic arborization neurons in Drosophila larva. *Brain Struct. Funct.* **223**, 1107–1120 (2018).

28. L. Baltruschat, G. Tavosanis, H. Cuntz, A developmental stretch-and-fill process that optimises dendritic wiring. bioRxiv 2020.07.07.191064 [Preprint]. 7 July 2022. https://doi.org/10.1101/2020.07.07.191064.

29. H. Cuntz, F. Forstner, A. Borst, M. Häusser, One rule to grow them all: A general theory of neuronal branching and its practical application. *PLOS Comput. Biol.* **6**, e1000877 (2010).

30. A. Luczak, Spatial embedding of neuronal trees modeled by diffusive growth. *J. Neurosci. Methods* **157**, 132–141 (2006).

31. K. Sugimura, K. Shimono, T. Uemura, A. Mochizuki, Self-organizing mechanism for development of space-filling neuronal dendrites. *PLOS Comput. Biol.* **3**, e212 (2007).

32. S. Ganguly, O. Trottier, X. Liang, H. Bowne-Anderson, J. Howard, Morphology of fly larval class IV dendrites accords with a random branching and contact based branch deletion model. arXiv:1611.05918 [q-bio.NC] (17 November 2016).

33. A. Palavalli, N. Tizón-Escamilla, J.-F. Rupprecht, T. Lecuit, Deterministic and stochastic rules of branching govern dendrite morphogenesis of sensory neurons. *Curr. Biol.* **31**, 459–472.e4 (2021).

34. R. J. Metzger, O. D. Klein, G. R. Martin, M. A. Krasnow, The branching programme of mouse lung development. *Nature* **453**, 745–750 (2008).

35. J. G. Lefevre, K. M. Short, T. O. Lamberton, O. Michos, D. Graf, I. M. Smyth, N. A. Hamilton, Branching morphogenesis in the developing kidney is governed by rules that pattern the ureteric tree. *Development* **144**, 4377–4385 (2017).

36. K. M. Short, A. N. Combes, J. Lefevre, A. L. Ju, K. M. Georgas, T. Lamberton, O. Cairncross, B. A. Rumballe, A. P. McMahon, N. A. Hamilton, I. M. Smyth, M. H. Little, Global quantification of tissue dynamics in the developing mouse kidney. *Dev. Cell* **29**, 188–202 (2014).

37. L. Kanari, P. Dłotko, M. Scolamiero, R. Levi, J. Shillcock, K. Hess, H. Markram, A topological representation of branching neuronal morphologies. *Neuroinformatics* **16**, 3–13 (2018).

38. E. Hannezo, C. L. G. J. Scheele, M. Moad, N. Drogo, R. Heer, R. V. Sampogna, J. van Rheenen, B. D. Simons, A unifying theory of branching morphogenesis. *Cell* **171**, 242–255.e27 (2017).

39. W. B. Grueber, L. Y. Jan, Y. N. Jan, Tiling of the Drosophila epidermis by multidendritic sensory neurons. *Development* **129**, 2867–2878 (2002).

40. W.-K. Yang, C.-T. Chien, Beyond being innervated: The epidermis actively shapes sensory dendritic patterning. *Open Biol.* **9**, 180257 (2019).

41. A. F. Castro, L. Baltruschat, T. Stürner, A. Bahrami, P. Jedlicka, G. Tavosanis, H. Cuntz, Achieving functional neuronal dendrite structure through sequential stochastic growth and retraction. *eLife* **9**, e60920 (2020).

42. F.-B. Gao, J. E. Brenman, L. Y. Jan, Y. N. Jan, Genes regulating dendritic outgrowth, branching, and routing in *Drosophila*. *Gene Dev.* **13**, 2549–2561 (1999).

43. J. D'Errico, SLM-shape language modeling (MathWorks, 2021); www.mathworks.com/matlabcentral/fileexchange/24443-slm-shape-language-modeling.

44. T. Mitchison, M. Kirschner, Dynamic instability of microtubule growth. *Nature* **312**, 237–242 (1984).

45. M. Dogterom, S. Leibler, Physical aspects of the growth and regulation of microtubule structures. *Phys. Rev. Lett.* **70**, 1347–1350 (1993).

46. M. Liao, X. Liang, J. Howard, The narrowing of dendrite branches across nodes follows a well-defined scaling law. *Proc. Natl. Acad. Sci. U.S.A.* **118**, e2022395118 (2021).

47. K. Falconer, *Fractal Geometry: Mathematical Foundations and Applications* (Wiley, ed. 2, 1990).

48. M. Kirschner, T. Mitchison, Beyond self-assembly: From microtubules to morphogenesis. *Cell* **45**, 329–342 (1986).

49. J. Toner, Y. Tu, Long-range order in a two-dimensional dynamical XY model: How birds fly together. *Phys. Rev. Lett.* **75**, 4326–4329 (1995).

50. T. Vicsek, A. Czirók, E. Ben-Jacob, I. Cohen, O. Shochet, Novel type of phase transition in a system of self-driven particles. *Phys. Rev. Lett.* **75**, 1226–1229 (1995).

51. S. R. Cajal, Histology of the nervous system of man and vertebrates, in *History of Neuroscience* (Oxford Univ. Press, 1995).

52. M. C. Uçar, D. Kamenev, K. Sunadome, D. Fachet, F. Lallemend, I. Adameyko, S. Hadjab, E. Hannezo, Theory of branching morphogenesis by local interactions and global guidance. *Nat. Commun.* **12**, 6830 (2021).

53. P. Lu, Z. Werb, Patterning mechanisms of branched organs. *Science* **322**, 1506–1509 (2008).

54. J. DeFelipe, P. L. López-Cruz, R. Benavides-Piccione, C. Bielza, P. Larrañaga, S. Anderson, A. Burkhalter, B. Cauli, A. Fairén, D. Feldmeyer, G. Fishell, D. Fitzpatrick, T. F. Freund, G. González-Burgos, S. Hestrin, S. Hill, P. R. Hof, J. Huang, E. G. Jones, Y. Kawaguchi, Z. Kisvárday, Y. Kubota, D. A. Lewis, O. Marín, H. Markram, C. J. McBain, H. S. Meyer, H. Monyer, S. B. Nelson, K. Rockland, J. Rossier, J. L. R. Rubenstein, B. Rudy, M. Scanziani, G. M. Shepherd, C. C. Sherwood, J. F. Staiger, G. Tamás, A. Thomson, Y. Wang, R. Yuste, G. A. Ascoli, New insights into the classification and nomenclature of cortical GABAergic interneurons. *Nat. Rev. Neurosci.* **14**, 202–216 (2013).

55. E. W. Dent, S. L. Gupton, F. B. Gertler, The growth cone cytoskeleton in axon outgrowth and guidance. *Cold Spring Harb. Perspect. Biol.* **3**, a001800 (2011).

56. X. Liang, M. Kokes, R. D. Fetter, M. D. Sallee, A. W. Moore, J. L. Feldman, K. Shen, Growth cone-localized microtubule organizing center establishes microtubule orientation in dendrites. *eLife* **9**, e56547 (2020).

57. C. Yalgin, S. Ebrahimi, C. Delandre, L. F. Yoong, S. Akimoto, H. Tran, R. Amikura, R. Spokony, B. Torben-Nielsen, K. P. White, A. W. Moore, Centrosomin represses dendrite branching by orienting microtubule nucleation. *Nat. Neurosci.* **18**, 1437–1445 (2015).

58. A. T. Weiner, M. C. Lanz, D. J. Goetschius, W. O. Hancock, M. M. Rolls, Kinesin-2 and Apc function at dendrite branch points to resolve microtubule collisions. *Cytoskeleton* **73**, 35–44 (2016).

59. M. Winding, M. T. Kelliher, W. Lu, J. Wildonger, V. I. Gelfand, Role of kinesin-1-based microtubule sliding in *Drosophila* nervous system development. *Proc. Natl. Acad. Sci. U.S.A.* **113**, E4985–E4994 (2016).

60. F. Decker, D. Oriola, B. Dalton, J. Brugués, Autocatalytic microtubule nucleation determines the size and mass of *Xenopus laevis* egg extract spindles. *eLife* **7**, e31149 (2018).

61. S. Petry, A. C. Groen, K. Ishihara, T. J. Mitchison, R. D. Vale, Branching microtubule nucleation in Xenopus egg extracts mediated by augmin and TPX2. **152**, 768–777 (2013).

62. T. D. Pollard, G. G. Borisy, Cellular motility driven by assembly and disassembly of actin filaments. *Cell* **112**, 453–465 (2003).

63. Y. A. Komarova, I. A. Vorobjev, G. G. Borisy, Life cycle of MTs: Persistent growth in the cell interior, asymmetric transition frequencies and effects of the cell boundary. *J. Cell Sci.* **115**, 3527–3539 (2002).

64. A. L. Arthur, S. Z. Yang, A. M. Abellaneda, J. Wildonger, Dendrite arborization requires the dynein cofactor NudE. *J. Cell Sci.* **128**, 2191–2201 (2015).

65. M. T. Kelliher, Y. Yue, A. Ng, D. Kamiyama, B. Huang, K. J. Verhey, J. Wildonger, Autoinhibition of kinesin-1 is essential to the dendrite-specific localization of Golgi outposts. *J. Cell Biol.* **217**, 2531–2547 (2018).

66. M. P. Forrest, E. Parnell, P. Penzes, Dendritic structural plasticity and neuropsychiatric disease. *Nat. Rev. Neurosci.* **19**, 215–234 (2018).

67. A. J. Koleske, Molecular mechanisms of dendrite stability. *Nat. Rev. Neurosci.* **14**, 536–550 (2013).

68. V. A. Kulkarni, B. L. Firestein, The dendritic tree and brain disorders. *Mol. Cell. Neurosci.* **50**, 10–20 (2012).

69. L. C. Kapitein, C. C. Hoogenraad, Building the neuronal microtubule cytoskeleton. *Neuron* **87**, 492–506 (2015).

70. A. O. Demchouk, M. K. Gardner, D. J. Odde, Microtubule tip tracking and tip structures at the nanometer scale using digital fluorescence microscopy. *Cell Mol. Bioeng.* **4**, 192–204 (2011).

71. F. Ruhnow, D. Zwicker, S. Diez, Tracking single particles and elongated filaments with nanometer precision. *Biophys. J.* **100**, 2820–8 (2011).

72. M. B. Smith, H. Li, T. Shen, X. Huang, E. Yusuf, D. Vavylonis, Segmentation and tracking of cytoskeletal filaments using open active contours. *Cytoskeleton* **67**, 693–705 (2010).

73. M. H. Longair, D. A. Baker, J. D. Armstrong, Simple Neurite Tracer: Open source software for reconstruction, visualization and analysis of neuronal processes. *Bioinformatics* **27**, 2453–2454 (2011).

74. P. C. Hansen, D. P. O'Leary, The use of the L-curve in the regularization of discrete Ill-Posed problems. *Siam. J. Sci. Comput.* **14**, 1487–1503 (1993).

75. R. A. Masri, K. A. Percival, A. Koizumi, P. R. Martin, U. Grünert, Survey of retinal ganglion cell morphology in marmoset. *J. Comp. Neurol.* **527**, 236–258 (2019).

76. S. Murru, S. Hess, E. Barth, E. R. Almajan, D. Schatton, S. Hermans, S. Brodesser, T. Langer, P. Kloppenburg, E. I. Rugarli, Astrocyte-specific deletion of the mitochondrial m-AAA protease reveals glial contribution to neurodegeneration. *Glia* **67**, 1526–1541 (2019).

77. S. Bloomfield, R. Miller, A functional organization of ON and OFF pathways in the rabbit retina. *J. Neurosci.* **6**, 1–13 (1986).

78. Z. Liu, R. Steward, L. Luo, Drosophila Lis1 is required for neuroblast proliferation, dendritic elaboration and axonal transport. *Nat. Cell Biol.* **2**, 776–783 (2000).